Analytical derivation of seismic fragility curves for historical masonry structures based on stochastic analysis of uncertain material parameters

Savvas Saloustros[a*], Luca Pelà[a], Francesca R. Contrafatto[a], Pere Roca[a], Ioannis Petromichelakis[b]

[a] Universitat Politècnica de Catalunya (UPC-BarcelonaTech), Department of Civil and Environmental Engineering, Jordi Girona 1-3, 08034 Barcelona, Spain

[b] Department of Civil Engineering and Engineering Mechanics, Columbia University, New York, USA

Abstract – This work presents a probabilistic method to assess the seismic vulnerability of historical masonry structures, such as churches or cathedrals, including uncertainty analysis of the material parameters. The proposed approach considers the pushover analysis using the finite element method for the structural evaluation of the seismic behaviour of masonry structures. A stochastic analysis based on Monte Carlo simulation investigates the effect of the uncertainty of the structural members' mechanical parameters on the evaluation of the seismic fragility. The method is applied to the seismic assessment of the bay structure of Santa Maria del Mar church in Barcelona, Spain. This case study is characterised by complex geometry and material heterogeneity, and shows to be sensitive enough to the uncertainty of the material properties to experience two possible collapse mechanisms in case of an earthquake. The study presents how to derive analytical seismic fragility curves by considering the uncertainties regarding the material properties and the different types of collapse mechanism.

Keywords: Monte Carlo simulation, Stochastic Analysis, Seismic Fragility Curves, Pushover Analysis, Finite Element Analysis, Masonry Church, Gothic.

---

[*] Corresponding author.

E-mail addresses: savvas.saloustros@upc.edu (Savvas Saloustros), luca.pela@upc.edu (Luca Pelà), contrafattofrancesca@tiscali.it (Francesca R. Contrafatto), pere.roca.fabregat@upc.edu (Pere Roca), ip2315@columbia.edu (Ioannis Petromichelakis)

1. Introduction

The evaluation of the seismic vulnerability of historical masonry buildings is a task of paramount importance nowadays. Such structures have shown to be very susceptible to damage and even to collapse in case of earthquakes, as demonstrated by the recent events in Europe, like the 2016-2017 Amatrice-Visso-Norcia seismic sequence in the central Italy.

Reliable methodologies able to deal with this problem are necessary especially for built cultural heritage masonry structures in order to ensure their conservation. This category of buildings usually includes complex structural typologies like churches, cathedrals, palaces and monuments. For these types of structures, seismic analysis is a very demanding task involving a high amount of uncertainty in the characterization of the geometry and complex morphology of the structural members, as well as the mechanical parameters of the constituent materials. This is true especially for historical masonry buildings, which present a significant variety of construction typologies and composite materials. The quality of historical masonry is related not only to the material constituents, but also to the constructive features such as the dimension of the blocks, bond, interlocking, and transversal connections. Much of this information, which would be essential for a reliable seismic analysis, is usually very difficult to acquire. The necessary inspection and experiments are often severely limited by their high cost and the restrictions posed by the cultural value of the buildings.

The evaluation of the seismic vulnerability of historical masonry structures still requires proper methodologies able to account for the variability of the structural and material

parameters affecting the seismic response of the structure. The limitations induced by the uncertainty of the materials' properties on conventional deterministic and semi-probabilistic approaches for seismic assessment are well known (Franchin, Pinto and Rajeev, 2010; Tondelli *et al.*, 2012). Another important source of uncertainty is due to the modelling hypotheses and adopted strategies for the analysis of the structure (Atamturktur, Hemez and Laman, 2012; Bracchi *et al.*, 2015)

Several European research projects have dedicated great attention to the problem of including the inherent probabilistic nature into the seismic risk assessment approach, such as RISK-UE, SYNER-G and PERPETUATE (Mouroux and Le Brun, 2006; Lagomarsino and Cattari, 2014b, 2014a). All these projects have developed different methodologies to derive seismic fragility functions for ordinary and cultural heritage masonry buildings, expressing the probability of occurrence of certain damage grades for different levels of seismic intensity.

The recent Italian guidelines CNR-DT 212/2013 (2014) have presented an organic methodology for the probabilistic vulnerability assessment of existing masonry buildings. The document suggests the derivation of analytical fragility curves as a function of the dispersion of the considered uncertain parameters.

Even though some authors have explored the effect of the uncertainty of material parameters in the probabilistic seismic assessment of masonry buildings (Rota, Penna and Magenes, 2010, 2014; Pagnini *et al.*, 2011; Snoj and Dolšek, 2011; Parisi and Augenti, 2012; Bosiljkov, D'Ayala and Novelli, 2015; Bracchi *et al.*, 2016), limited studies are available about the case of more complex structural typologies in historical constructions (Petromichelakis, Saloustros and Pelà, 2014; Bartoli *et al.*, 2017; Saloustros *et al.*, 2019).

This paper presents a probabilistic methodology for the analytical derivation of seismic fragility functions of complex masonry historical structures including the uncertainty regarding the materials' mechanical parameters. The approach makes use of the Finite Element Analysis (FEA) for the evaluation of the seismic structural capacity through nonlinear static (pushover) analysis. A stochastic nonlinear analysis based on Monte Carlo simulation allows the investigation of the effect of the material parameters' uncertainty on the evaluation of the seismic fragility.

The method is applied to the study of the church of Santa Maria del Mar in Barcelona, Spain. The paper evaluates the seismic vulnerability of the representative macro-element of the bay structure against transversal horizontal loading considering the uncertainties in the definition of the materials' mechanical properties. The uncertain material properties of the different structural members of the macro-element are considered as random variables with associated probability distributions and ranges of variation. The effect of these uncertainties is investigated by analysing 200 random samples of possible material combinations for the same structure by means of a Monte Carlo Simulation. The force-displacement capacity of the different models has been calculated by FEA on 200 pushover analyses. The application of the N2 method permits the evaluation of the seismic demand for the city of Barcelona corresponding to four damage limit states (slight, moderate, extensive and complete) for all the investigated cases. The derivation of analytical fragility curves allows the definition of the probability of occurrence of each damage grade for different seismic hazard scenarios. Due to the prediction of two different collapse mechanisms, fragility curves are derived either by separating the 200 analyses in two groups

depending on the predicted collapse mechanism or by using all the analyses without making any such differentiation. The effect of these alternatives on the estimation of the seismic fragility of the structure is discussed.

2. Proposed methodology for probabilistic seismic assessment including material uncertainty

This work proposes a methodology to evaluate analytical fragility curves in which the seismic vulnerability of a complex historical masonry building is evaluated taking into account the uncertainty of the materials' mechanical properties.

The first step of the procedure is to identify and characterize the uncertain data. This activity is the result of the analysis of the diverse material typologies existing in the different structural members composing the complex building. For this reason, it is important the level of knowledge of the investigated building, as derived from inspection, survey and, if possible, experimental testing.

Different mathematical models are available to assess the characteristics of uncertain parameters within a computational framework (Graf, Götz and Kaliske, 2015). The best compromise in terms of simplicity, reliability and computational efficiency lays in the concept of *random variables*, as derived from probability theory. The definition of a suitable probability density function for each random variable can model its uncertainty within reasonable ranges of variation.

The effect of the uncertainty of parameters on the seismic response of the investigated structure is evaluated by means of stochastic analysis. Among the available stochastic

methods, this paper considers a Monte Carlo Simulation due to its effectiveness and adequacy to structural problems, as suggested by previous works (Rota, Penna and Magenes, 2010; Pagnini *et al.*, 2011; Petromichelakis, Saloustros and Pelà, 2014) and relevant standards (CNR-DT 212/2013, 2014).

The Monte Carlo Simulation generates a specified number of *N* independent and identically distributed random samples (population of structural instances/cases to be analysed) within the input space $\boldsymbol{x} \subseteq \mathbb{R}^{\boldsymbol{n}}$, where *n* is the number of the assumed input random variables, i.e. the uncertain material parameters. The sampling process takes into account the probability distributions associated to each of the random variables. The selection of suitable probability density functions for the uncertain material parameters is based on recent studies for masonry structures (Sykora and Holicky, 2010; CNR-DT 212/2013, 2014) and the recommendations of technical codes (MIT, 2009; CNR-DT 212/2013, 2014).

Then, a mapping model maps each of the *N* samples to the result space $\boldsymbol{Z} \subseteq \mathbb{R}^{\boldsymbol{m}}$**,** where *m* is the number of the result variables to be evaluated. The mapping model proposed in this research includes the development of *N* pushover seismic analyses by FEA, the evaluation of the seismic performance by the N2 method (Fajfar, 1999) and the identification of the seismic demands associated to conveniently defined damage limit states. Finally, analytical seismic fragility curves are plotted as a function of the output variables. Figure 1 shows a flowchart summarizing the different stages of the proposed methodology.

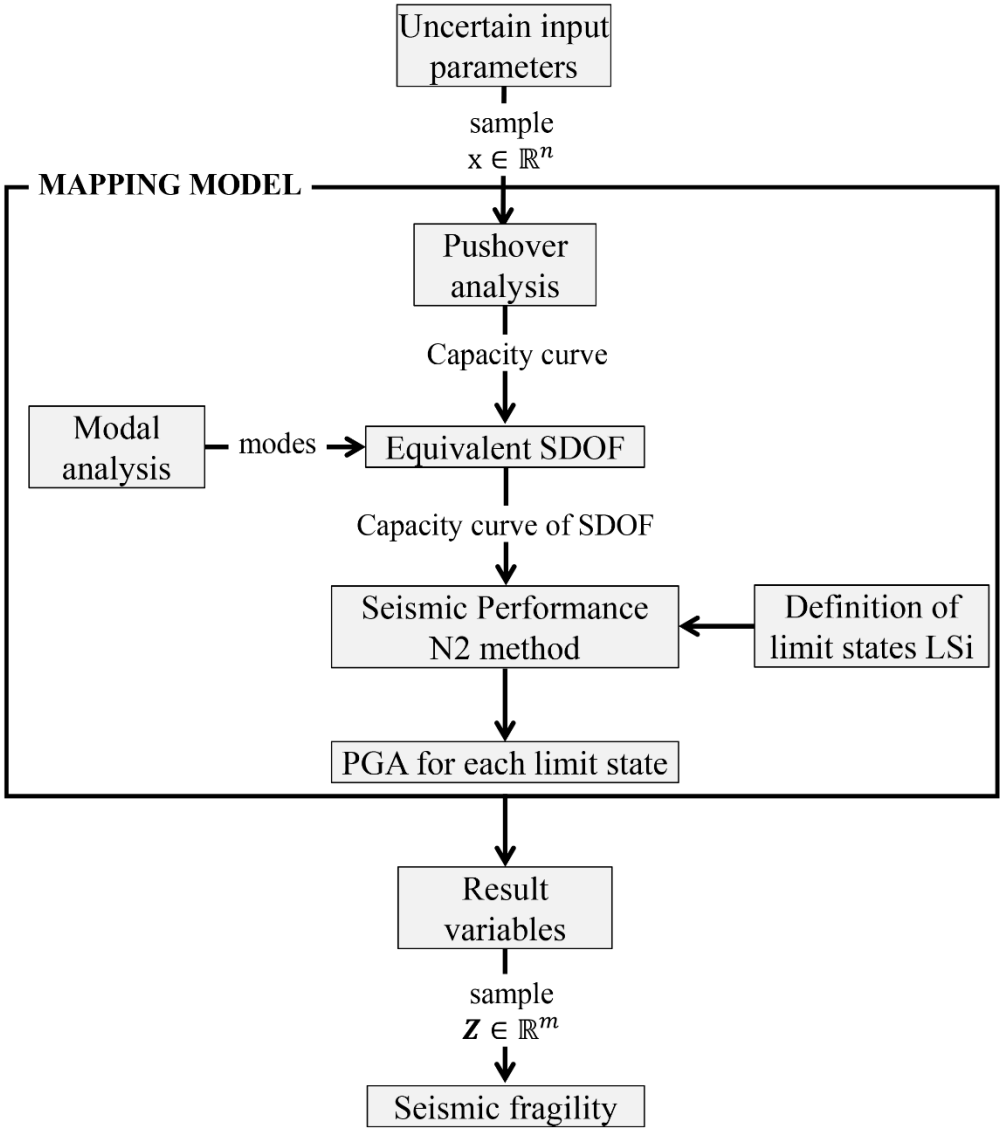

Figure 1. Scheme of the adopted methodology for the probabilistic assessment of the seismic vulnerability of masonry structures including material uncertainty.

3. The case study: church of Santa Maria del Mar, Barcelona

3.1 Description of the building and previous studies

The church of Santa Maria del Mar is located in the Ribera district of Barcelona, Spain. The remarkably short time of construction, begun in 1329 and lasting for only 53 years, constitutes a rare case for a Gothic church of such large dimensions and structural complexity. The structure, symmetrical with respect to the longitudinal axis (north-south direction), is 85 *m* long and 35.3 *m* wide, with a maximum height, up to the high vault keystones, of 34 *m*. The church is composed of three longitudinal naves, covered by square cross vaults, and a semi-circular apse at the north. The south façade includes two bell towers, an imposing rose window with a diameter of 9.0 *m* and two perpendicular buttresses counteracting the longitudinal thrust exerted by the first cross vault of the nave, see Figure 2. The church does not present a pitched roof, but a terrace with a tile pavement shaped over the cross vaults.

Octagonal columns, with circumscribed diameter of 1.6 *m* and height of 26.0 *m*, sustain the cross vaults of the church. Four square cross vaults spanning 13.5 *m* roof the central nave. They are stiffened at the extrados by diaphragmatic arches, aligned with the columns and the lateral wall-buttresses. Triangular walls built over the lateral cross vaults provide the continuity of diaphragmatic arches towards the buttresses. These triangular walls, built as part of the water drainage system, are also structurally relevant, especially under earthquake as shown by the studies carried out.

Smaller rectangular cross vaults cover the lateral naves of the church, with span half of that of the central cross vaults. Their height up to their keystones is 32 *m*, i.e. similar to

that of the central vaults to counteract their horizontal thrust and carry it to the buttresses. This architectural feature, typical of the Catalan Gothic architecture, makes the existence of flying arches unnecessary.

(a)

(b)

Figure 2. (a) Façade and (b) interior of Santa Maria del Mar church in Barcelona, Spain (photograph by (Mayer, 2008), distributed under a CC BY-SA 3.0 ES license).

A detailed survey and inspection campaign performed on site (Vendrell *et al.*, 2007) provided valuable information regarding the dimension and inner morphology of the structural members. Walls and buttresses are composed of three-leaves whose external layers are made of ashlar masonry with lime mortar joints, while the inner core consists of irregular rubble masonry. All the stone materials come from the quarries of Montjuïc hill in Barcelona. Sonic tomography carried out on the columns revealed the inner morphology of the octagonal piers, with rows consisting of four external hexagonal stones surrounding a square central one (González *et al.*, 2008). Each row is rotated 45º with respect to the inferior ones to provide interlocking between stone blocs. Compared to the rest of vertical load-bearing members, the piers can benefit from a higher strength and stiffness due to the large dimensions of the stones and the thinness of the mortar joints.

The vaults are made of stones of thickness of around 0.2 *m*. The lateral vaults present at the extrados a supplementary fill layer of load-carrying material consisting of rubble masonry bonded with lime mortar, a kind of medieval concrete. The central vaults are backed with rubble masonry and then supplemented, up to the terrace pavement level, with a light infill layer composed of ceramic empty pots bonded with lime mortar.

The church of Santa Maria del Mar experienced the effects of several earthquakes during its history (González *et al.*, 2008). According to available historical documents, an earthquake in 1373 caused the failure of the upper gallery of one of the bell towers , and another one in 1428 caused about twenty casualties due to the collapse of the rose window at the end of religious ceremony (Fontserè, 1971).

Several previous studies have investigated the seismic performance of Santa Maria del Mar. Within the RISK-UE project, Irizarry (2004) studied a transversal section of the

church, evaluating the structural capacity by Limit Analysis (LA) and Finite Element Analysis (FEA). In the framework of an interdisciplinary study done to assess the structural condition of the church, Vendrell et al. (2007) and Roca et al. (2009) carried out nonlinear seismic FEA on a 3D model representing a transversal bay of the church and LA on additional macro-elements involving the façade and the towers.

3.2 Finite Element model

The proposed probabilistic approach is applied in this research for the evaluation of the seismic response along the transversal (east-west) direction of the representative bay structure of Santa Maria del Mar, including the main and lateral naves. The geometry of the macro-element has been extracted from a Laser Scanner survey of the entire building (Figure 3).

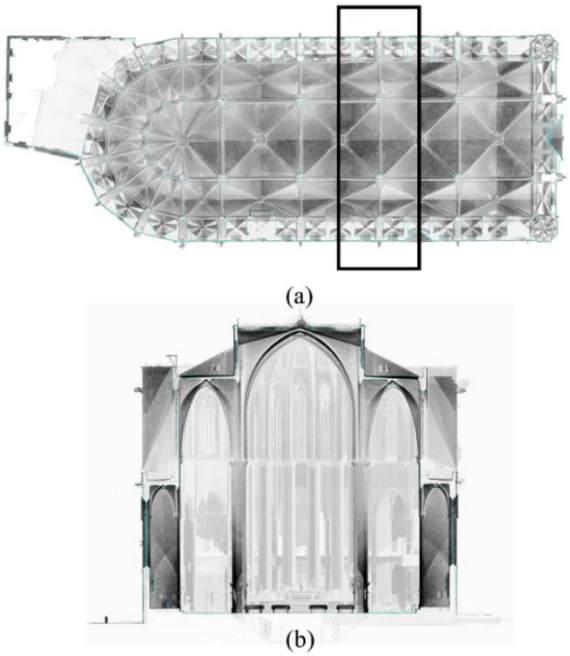

Figure 3. Presentation of the selected macro-element of the Santa Maria del Mar church in Barcelona as a cloud of points obtained through laser scanner survey: (a) floor of the structure with the transversal bay in rectangle, (b) the selected transversal section.

The selected macro-element is represented numerically as a two-dimensional finite element model. Figure 4 presents the finite element mesh, composed of 37780 triangular constant strain plane stress finite elements and 17749 nodes. The mesh is refined in the parts of the structure where high stress gradients commonly occur, such as the vaults and the buttresses. Numerical analysis are performed by using the finite element code DIANA-FEA (TNO, 2017) and the mechanical response of masonry is simulated adopting the total strain rotating crack model. The nonlinear post-peak compressive behaviour is characterized by a parabolic stress-strain relationship, whereas the tensile one by exponential softening. The stress-strain relationships are regularized according to the crack-bandwidth approach (Bažant and Oh, 1983), ensuring mesh-size independent results.

The numerical model has been calibrated following a two-step procedure. The first step includes its comparison with a detailed 3D finite element model of the same macro-element (Murcia, 2008; Roca *et al.*, 2009), such that the two models present an equivalent response in terms of stiffness and capacity under both gravitational and horizontal in-plane loading proportional to the mass distribution. The second-step considers the comparison of the numerical vibration characteristics with the results of the experimental dynamic identification reported in (Vendrell *et al.*, 2007). The fundamental vibration mode predicted by the numerical analysis in the transversal direction of the church has an eigen-frequency of 1.39 Hz and a participating mass of 70.6% (Figure 5), while the second numerical eigen-frequency in the same direction is 7.02 Hz, with a participating mass of 9.2%. The first numerical eigen-frequency is 5% lower than the experimental one, measured equal to 1.45 Hz.

The adopted calibration methodology of the numerical model, which has been used for similar historical churches (Roca *et al.*, 2013; Petromichelakis, Saloustros and Pelà, 2014), has been detailed for the selected macro-element of Santa Maria del Mar church in Contrafatto (2017). The choice of a simplified two-dimensional model allows the execution of the large number of numerical simulations required by the probabilistic approach at an affordable computational cost.

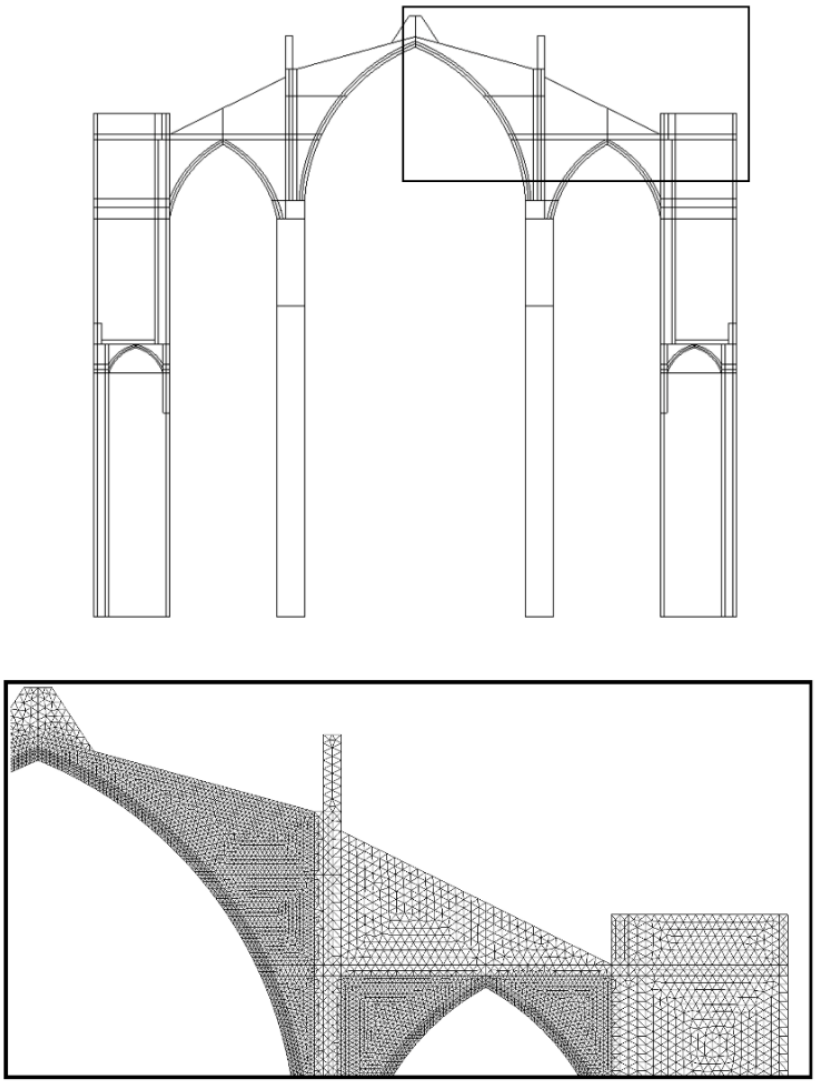

Figure 4. Numerical model of the transversal bay of the church of Santa Maria del Mar with a close-up of the adopted mesh at the top part of the structure.

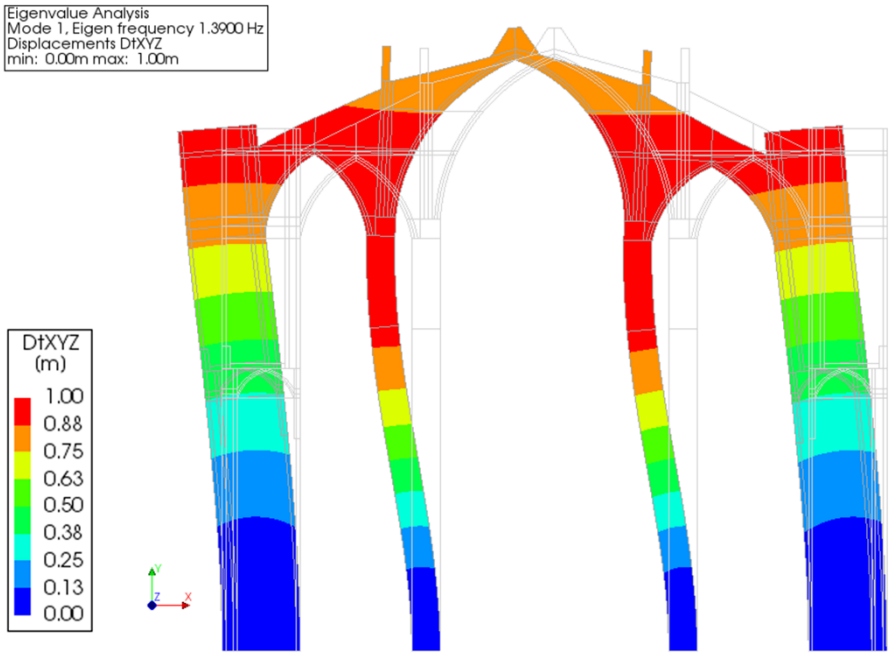

Figure 5. First vibration modal shape of the investigated macro-element.

Equivalent non-linear static (pushover) analyses are used to study the effect of seismic actions on the selected macro-element, according to available standards (EN 1998-1 (Eurocode 8) 2003; CNR-DT 212/2013 2014). The first stage of each analysis includes the application of the vertical gravitational loads, and the second one corresponds to the application of the seismic horizontal load proportional to the mass orthogonally to the longitudinal direction of the church. The geometrical and material non-linear problem is solved though a regular Newton Raphson method with an arc-length strategy. Convergence is checked based on force and displacement norm ratios below 1%.

3.3 Random variables

Based on available studies on the construction materials of the church (Vendrell *et al.*, 2007), the structural elements are classified into four categories of materials with similar

mechanical properties. These are the vaults and single-leaf walls (group I), the three-leaf walls with the heavy infill (group II), the columns (group III) and the light vault infill (group IV), shown in Figure 6.

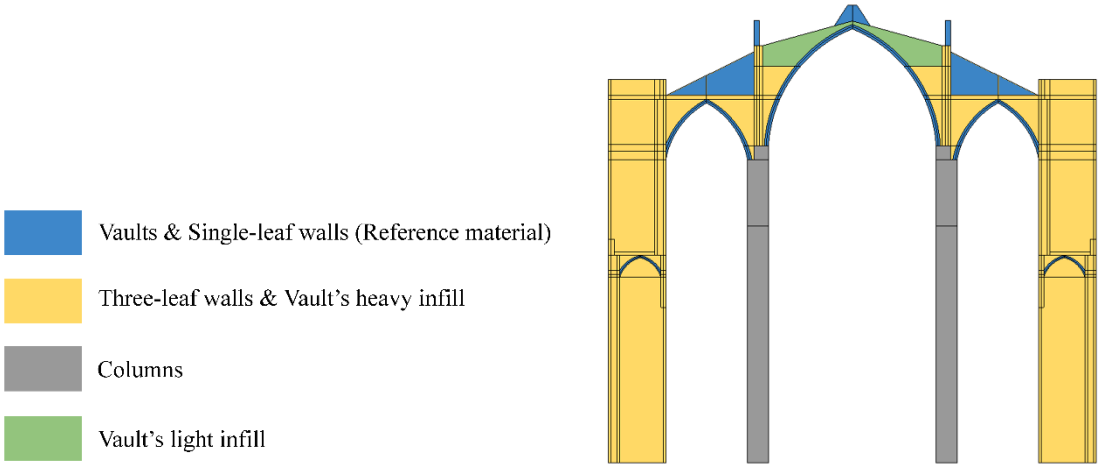

Figure 6. Classification of the structural members into four categories according to the mechanical properties of materials.

The probabilistic analysis considers the vaults and the single-leaf walls (group I) as the "reference material", and six material parameters as random variables. Three of them are the mechanical properties of the reference material, namely the compressive strength f_c, the tensile strength f_t, and the Young's modulus E. These material properties are characterized by aleatoric and epistemic uncertainty. The aleatoric uncertainty is due to the natural variation of the mechanical properties of masonry. The epistemic uncertainty is attributed to the impossibility to achieve a complete knowledge of the variation of the mechanical properties of masonry within existing structures. The values of these three parameters are defined to vary according to a lognormal probability density function, in agreement with references (Park *et al.*, 2009; CNR-DT 212/2013, 2014). The statistical

description of these parameters has been defined through the following procedure. Each of the four categories of materials shown in Figure 6 is associated to a masonry typology described in Table C8A.2.1 of the Instructions to Italian standards (MIT, 2009). In particular, making reference to the Table C8A.2.1 of (MIT, 2009), the properties of group I and group III are defined according to the 5th masonry typology ("squared stone masonry"). Despite being associated to the same masonry typology, group III presents higher mechanical properties compared to group I, due to the thin mortar joints and the good interlocking between the stone block in the columns, which was confirmed by sonic tomography tests (Vendrell *et al.*, 2007). For this reason, a correction factor of 1.2 has been applied to the mechanical properties of group III following the suggestions of Table C8A.2.2 in (MIT, 2009). Regarding the material properties of the three-leaf walls and the vaults' infill (Group II), these are assumed to fall within the limits of the 2nd masonry typology ("roughly cut stone masonry, having wythes of limited thickness and inner core") in Table C8A.2.2 in (MIT, 2009). In this case, two correction coefficients have been applied following the suggestions of Table C8A.2.2 in (MIT, 2009) due to the good bonding transversal connection between the external leaves (correction factor of 1.5) and the good mortar quality (correction factor of 1.4). Finally, the properties of the vaults' light infill have been defined according the values proposed for the 1st masonry typology ("irregular stone masonry") in Table C8A.2.2 in (MIT, 2009). This procedure, based on the existing information of materials presented in Section 3.1 and following the suggestions of Tables C8A.2.1 - C8A.2.2 of the Instructions to Italian standards (MIT, 2009) permits a first estimation of the range of variation for the compressive strength, presented in Table 1.

Table 1. Estimation of the lower and upper bounds for the compressive strength of the different material groups following the procedure proposed in (MIT, 2009).

	Compressive strength fc [MPa]	
Material Group	Lower Bound	Upper Bound
Group I Vaults & single-leaf walls	6.0	8.0
Group II Three-leaf walls & vault's heavy infill	7.2	9.6
Group III Columns	4.2	6.3
Group IV Vault's light infill	1.0	1.8

Following the above procedure, the value of the standard deviation (Table 2), is defined such that the great majority of the selected population of the compressive strength falls within the upper and lower bounds shown in Table 1. Figure 7 shows that for the performed Monte Carlo simulation the 100% of the values of compressive strength are bounded by the lower and upper bounds suggested by (MIT, 2009), i.e. 6.0 MPa and 8.0 MPa. The Young's modulus is related to the compressive strength as E/f_c=300÷500. These limit values are also consistent with the range of variation reported for the selected masonry typologies in Table C8A.2.1 of (MIT, 2009), despite the variability found in the literature (Vanin *et al.*, 2017). In fact, the suggested ratio E/f_c is 400 for the 5th masonry typology ("squared stone masonry") in Table C8A.2.1 of (MIT, 2009). The tensile strength is also related to the compressive strength with limits assumed in the range f_t/f_c=0.02÷0.05 according to previous studies by the authors on similar stone masonry typologies (Roca *et al.*, 2013; Saloustros *et al.*, 2014; Pelà *et al.*, 2016). Similarly to the compressive strength, the values of the standard deviation of the lognormal distributions

of Young's modulus and tensile strength (Table 2) have been defined such that the majority of the values falls within the defined lower and upper bounds, see Figure 7.

Table 2. Probability distributions and their parameters for the compressive strength, tensile strength and Young's modulus of the reference material (vaults and single-leaf walls).

Random variable	Probability Distribution	Mean μ [MPa]	Lognormal mean μ_{ln}	Standard deviation σ_{ln}
f_c	lognormal	7.00	1.94	0.05
f_t	lognormal	0.26	-1.37	0.22
E	lognormal	2900	7.96	0.13

The compressive strength, the Young's modulus and the tensile strength for the other three categories of materials (groups II, III, and IV) are defined as proportional to that of the reference material. The proportionality coefficients are denoted by W_c for the three-leaf walls and the vaults' heavy infill (Group II), C_c for the columns (Group III) and I_c for the vaults' light infill (Group IV). These coefficients are characterised by only epistemic uncertainty, and their assessment is linked to the uncertainty of the assumed model, as well as to the state of knowledge. Regarding the relationship between the mechanical parameters of different groups of materials, only rough estimations about the variation intervals are possible. For this reason, the variation of the above coefficients of proportionality follows a uniform distribution. Table 3 presents the minimum and maximum values for the coefficients W_c, C_c and I_c. Similar to the reference material, these are selected such that the possible values of the material parameters follow the suggestions of (MIT, 2009) . It is worth noting that the use of the proportionality coefficients W_c, C_c and

I_c entails that any random sample generated by the Monte Carlo simulation presents the same E/f_c and f_t/f_c relationships in all material categories (groups I-IV).

Table 3 Ranges of variation for the proportionality coefficients C_c, W_c and I_c establishing the relationship between the mechanical properties of the reference materials and the others.

Random variable	Distribution	Minimum	Maximum
C_c	uniform	0.7	0.8
W_c	uniform	1.1	1.3
I_c	uniform	0.17	0.23

Table 4 Mean values of the mechanical properties used in the reference model.

Structural Element	f_c [MPa]	f_t [MPa]	E [MPa]	G_f^t $[J/m^2]$	G_f^c $[J/m^2]$
Vaults and single-leaf walls	7.00	0.26	2900	19.5	11200
Three-leaf walls & heavy infill vaults	5.30	0.20	2230	16.0	8480
Columns	8.50	0.33	3590	22.3	13600
Light infill vaults	1.43	0.06	613	6.4	2288

The tensile and compressive fracture energy for all the materials have been defined as a function of the compressive strength f_c as $G_f^t = 0.025(f_c/10)^{0.7}$ and $G_f^c = df_c$ according to CEB-FIP (2013) and Lourenço (2009), respectively. The ductility index in the equation of the compressive fracture energy is defined as $d = 1.6\ mm$ (Lourenço, 2009). Due to the lack of experimental data for the investigated structure, the correlation between the mechanical properties of a material is based on technical codes (MIT, 2009; CEB-FIP, 2013) and expert judgement. In the presence of experimental data, a comprehensive statistical analysis could be followed for an accurate characterization of the correlation structure between the chosen random variables as in (Franchin *et al.*, 2018).

Table 4 presents the mean values for the different materials. These values, which represent a plausible choice in the absence of experimental data, define the properties of the "reference model", i.e. the combination of values for the mechanical parameters that might be considered in a conventional deterministic or semi-probabilistic approach to the problem. The outcome from the reference model will be compared with the results from the probabilistic analysis proposed in this work.

3.4 Uncertainty analysis of material parameters

The Monte Carlo stochastic simulation developed for the analysis of Santa Maria del Mar has created a population of N = 200 structural cases for the selected structural macro-element. These N cases correspond to the execution of 200 different seismic pushover analyses by means of the finite element method. The selected number of the sample size is based on the past experience of the authors in analysing similar structures (Petromichelakis, Saloustros and Pelà, 2014) and in accordance with previous studies in the field by Vamvatsikos and Fragiadakis (2010) and Jalayer, Iervolino and Manfredi, (2010). Section 4.3 presents the analysis of the effect of the choice of the sample size, showing that the chosen one of N=200 seems to be appropriate for the selected case study. The number of random variables in this study is n = 6 due to the assumptions made in Section 3.3. Figure 7 illustrates the distribution of the three first random variables for the reference material, i.e. the compressive strength, the tensile strength and the Young's modulus. These plots give an additional indication that the selected sample size is sufficient to give an input that converges to the lognormal distributions with the statistical parameters of Table 2.

The number of results variables is $m = 4$, corresponding to the seismic demand values, expressed in terms of Peak Ground Acceleration (PGA), associated to each of the four limit states that will be defined in the next Section 3.5.

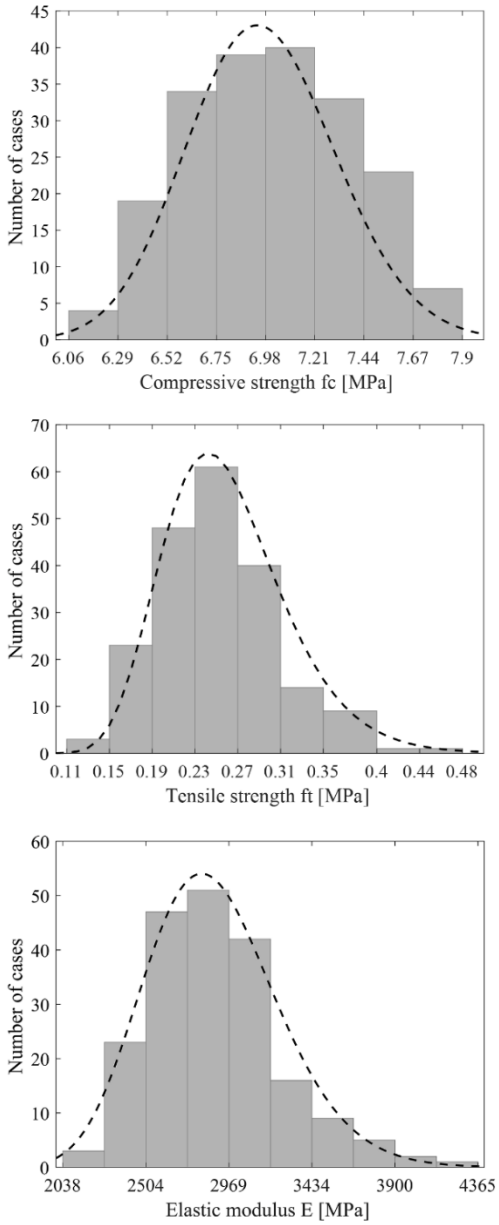

Figure 7. Histograms with the distributions of selected values for the compressive strength f_c (top) the tensile strength f_t, (middle) and the elastic modulus E (bottom) and corresponding lognormal probability density functions (in dashed line) for the reference material.

3.5 Damage limit states and seismic demand

The seismic vulnerability of the selected macro-element is related to the probability of the structure to reach different *limit states*. Each of these limit states, denoted as LS_i, represents distinct damaged states of the structure corresponding to different seismic demands, expressed in terms of spectral displacements of the equivalent Single Degree Of Freedom System (SDOF). This works defines the limit states by adopting the definitions proposed by Lagomarsino & Giovinazzi (2006) for masonry buildings. According to these authors, four limit states are considered as a function of the yield displacement d_y and the ultimate displacement d_u of the idealized capacity curve corresponding to the equivalent SDOF. The latter curve is constructed according to the Italian Ministry of Infrastructure and Transport (2009) by considering the ultimate displacement as the one corresponding to a decrease of 20% of the maximum load capacity of the structure. Table 5 presents the definition of each limit state and their association with the damage state of the structure. It is noted that the definition of the limit states for complex masonry structural typologies, as the one studied in this work, is still an open issue. Different approaches relating the limit states with the cracking affecting the investigated structure or the formation of the collapse mechanism have been presented in previous studies (Lagomarsino and Resemini, 2009; Petromichelakis, Saloustros and Pelà, 2014; Ortega *et al.*, 2018).

Table 5. Definition of the limit states and their correspondence with the damage states of the structure (d_y and d_u stand for the yield and ultimate displacement of the equivalent Single Degree Of Freedom System - SDOF) according to Lagomarsino & Giovinazzi (2006)

Limit State	Displacement of the equivalent SDOF	Damage state
LS_1	0.7 d_y	Slight
LS_2	1.5 d_y	Moderate
LS_3	0.5 (d_y + d_u)	Extensive
LS_4	d_u	Complete

The Peak Ground Acceleration (PGA) corresponding to each limit state is identified through the N2 method (Fajfar, 1999), in agreement with the Annex B of EN 1998-1 (Eurocode 8, 2003) and several cases in the existing literature dealing with masonry structures (D'Ayala and Ansal, 2012; Acito *et al.*, 2014; Simões *et al.*, 2015; Castellazzi *et al.*, 2017). The elastic spectrum is defined according to the Eurocode 8 by considering the type of soil of the area. An available geotechnical study (Vendrell *et al.*, 2007), carried out in the surrounding of the church, revealed the existence of a layer of poor quality rubble material of anthropogenic origin. Due to this, a Soil Type D is used for the definition of the elastic spectrum according to the Eurocode 8. Figure 8 illustrates the application of the N2 method for a capacity curve obtained for one of the studied cases. As soon as the limit states have been identified for each curve (shown with dots in Figure 8), the N2 method allows the identification of the corresponding seismic demand for each of them in terms of Peak Ground Acceleration.

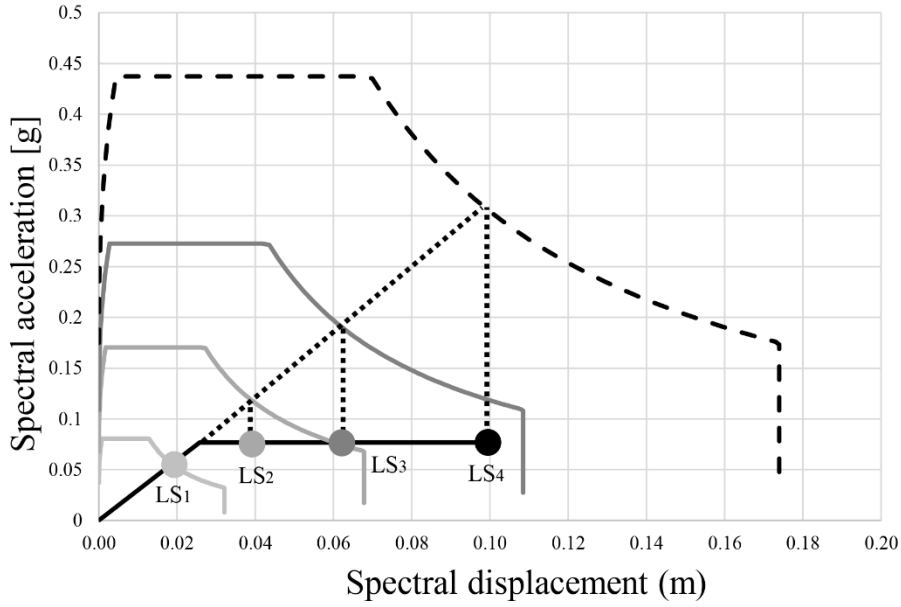

Figure 8. Illustration of the application of the N2 method for obtaining the seismic demand in terms of PGA for the four limit states.

3.6 Seismic Fragility

The seismic fragility of the analysed macro-element of Santa Maria del Mar church is expressed in terms of analytical fragility curves, representing the probability that the structure will exceed each considered damage limit state LS_i as a function of the PGA. This work considers the fragility function generally accepted in available standards (ATC-58, 2009; Federal Emergency Management Agency, 2010), i.e. the log-normal cumulative distribution function. According to the latter, the conditional probability of being in, or exceeding, a particular limit state LS_i, given a value of PGA, is

$$P[LS_i|PGA] = \Phi\left[\frac{1}{\beta_{LS_i}} ln\left(\frac{PGA}{\theta_{LS_i}}\right)\right]. \quad (1)$$

where θ_{LS_i} is the median value of the PGA at which the analysed macro-element reaches the limit state LS_i, β_{LS_i} is the standard deviation of the natural logarithm of the PGA for

limit state LS_i and Φ is the standard normal cumulative distribution function. The above values of θ_{LS_i} and β_{LS_i} are computed through the following functions

$$\theta_{LS_i} = e^{\left(\frac{1}{N}\sum_{j=1}^{N} \ln PGA_j\right)} \approx PGA_{50\%} \tag{2}$$

$$\beta_{LS_i} = \sqrt{\frac{1}{N-1}\sum_{j=1}^{N}\left(ln\left(\frac{PGA_j}{\theta_{LS_i}}\right)\right)^2} \tag{3}$$

where N is the selected number of structural samples analysed in the Monte Carlo stochastic simulation and $(PGA)_j$ is the Peak Ground Acceleration for the case $j = 1, N$.

4. Results

4.1 Seismic capacity curves

Figure 9 presents the results of the N=200 pushover analyses in terms of the horizontal acceleration against the horizontal displacement at the key of the vault in the main nave. It is easy to identify two groups of capacity curves with important differences in load and displacement capacities. The first group, composed by N_G = 163 cases, is characterized by load capacities ranging between 0.075 g and 0.11 g, and a more ductile post-peak response. The second group, composed of N_L = 37 cases, presents much lower load capacity levels, ranging between 0.03 g and 0.07 g, and a brittle post-peak response.

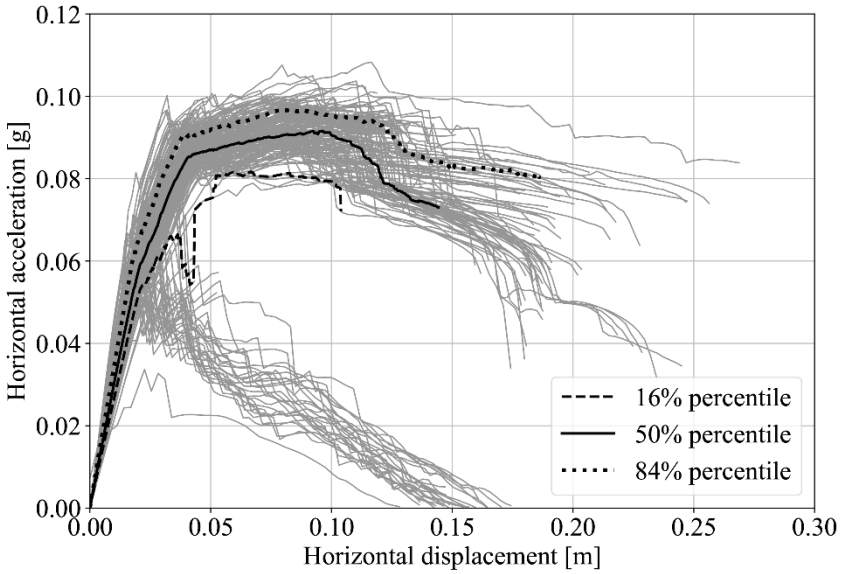

Figure 9. Capacity curves and 16%, 50% and 84% percentiles of the *N*=200 analysed cases in terms of horizontal load multiplier against horizontal displacement at the key of the vault in the central nave.

The presence of the two groups of the capacity curves in Figure 9 is due to the possibility of obtaining two different collapse mechanisms in the finite element analysis of the studied macro-element after varying the mechanical properties of the materials. The analysed cases falling within the group with higher capacity present a global collapse mechanism of the macro-element, shown in Figure 10a. For these cases, cracking at the main and lateral naves and at the two lateral buttresses provokes the global failure of the structure. Contrariwise, the second group with lower capacity is characterized by a local collapse mechanism of the analysed macro-element, as illustrated in Figure 10b, with the collapse of the right buttress due to shear cracking.

The three black lines in Figure 9 are the 16%, 50% and 84% percentile curves, representing for each displacement the horizontal acceleration that is not exceeded by the 16%,

50% and 84% of the analysed cases, respectively. Using the side percentile curves it is easy to identify that the large majority of the capacity curves falling above the 16% percentile curve, correspond to cases predicting a global collapse mechanism of the studied macro-element. Hence, the visual presentation of the side percentile curves in Figure 9 demonstrates that the structure is most likely (roughly 84% of probability) to present a global collapse mechanism for the investigated combination of material parameters. It is noted that these percentile curves are conventionally adopted also in FEMA (Federal Emergency Management Agency 2010), and have been derived considering all the samples.

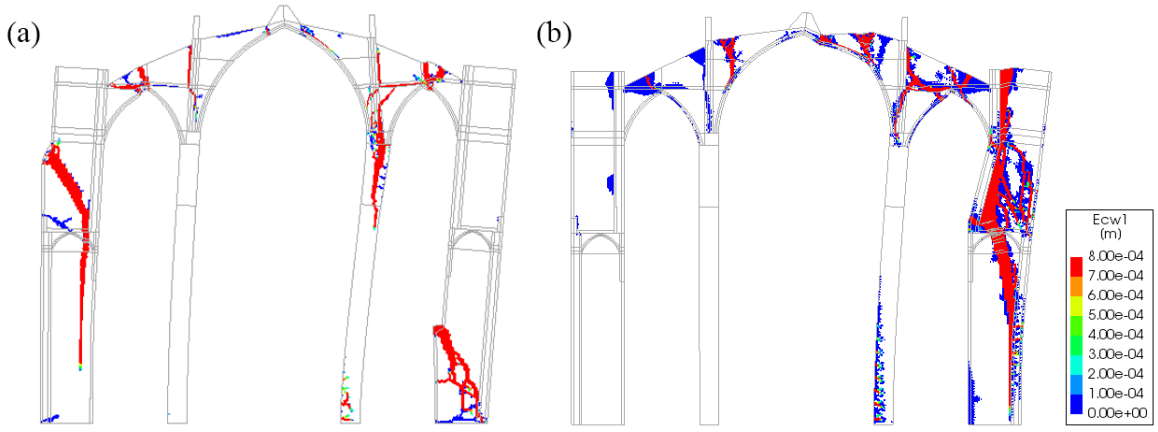

Figure 10. Contour of the crack widths for the two collapse mechanisms predicted by the pushover analyses after considering the variation of material parameters: (a) global mechanism involving the buttresses and the main and lateral naves, (b) local collapse of the right buttress.

Figure 11 presents the mean, the median and the pushover curve of the reference case. The latter corresponds to an analysis adopting as mechanical properties the mean values for each material category presented in Table 4 and obtained following the procedure described in Section 3.4. The mean curve represents the average acceleration of all the

analysed cases for each displacement level, while the median corresponds to the aforementioned 50% percentile curve. The higher position of the median curve compared to the mean one implies that for the adopted distributions of the uncertain parameters, the distribution of the horizontal acceleration for a given horizontal displacement is unsymmetrical and shifted to the higher values. In other words, for each value of the horizontal displacement the capacity curves below the median are located slightly farther from the median than the capacity curves above it. For the analysed structure, this happens due to the quite distinct response of the N_L cases predicting the local collapse mechanism, which increases the dispersion of the capacity curves, as can be seen in Figure 9. The above result suggests that samples with one or more input parameters below the mean, push the capacity curve downwards more than samples above the mean push it upwards. Consequently, the use of a single numerical model with deterministic mechanical properties, adopted following the suggested values from the literature, may predict a very different structural capacity compared to the average of the analysed cases. Due to this, the reference model predicts a higher capacity than that given by the mean and median curves, as shown in Figure 11. This implies that the use of a single numerical model with deterministic/semi-probabilistic mechanical properties from the literature would overestimate the structural capacity for the analysed case. This result underlines the importance of considering the uncertainties of the mechanical properties in the seismic assessment of complex masonry structures.

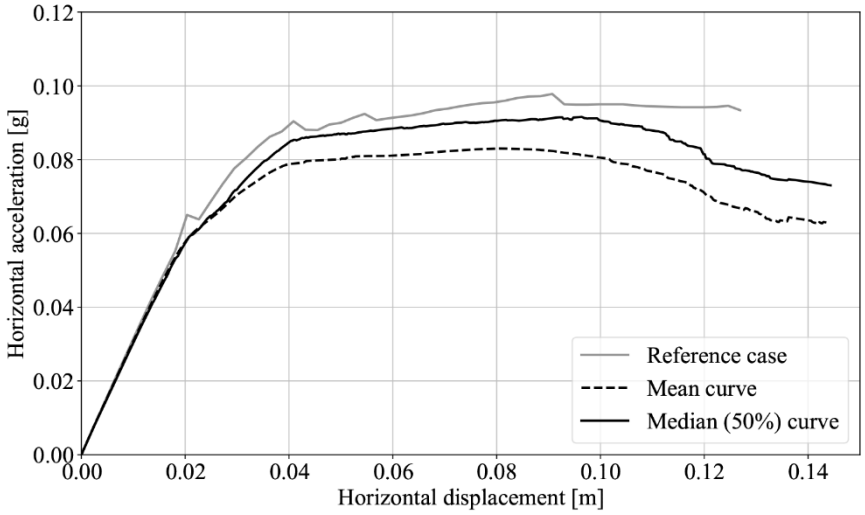

Figure 11. Mean, median capacity curves of the N = 200 analysed cases along with the capacity curve of a reference model using deterministic values of Table 4.

Figure 12a and Figure 12b present the mean and median capacity curves computed by considering only the results of the N_G and N_L cases predicting the global and the local collapse mechanisms of the selected macro-element, respectively. Considering only the cases leading to the same collapse mechanism minimizes the differences between the mean and the median capacity curves. This means that for both cases there is a very similar distribution of the horizontal accelerations around the mean value for each displacement level. Once again, the difference between the reference case (grey lines in Figure 12) and the average response of the analysed cases (dashed black line in Figure 12) demonstrates the potential erroneous estimation of the capacity of the structure by using a deterministic/semi-probabilistic approach. This difference becomes particularly important for the N_L cases, as illustrated in Figure 12b.

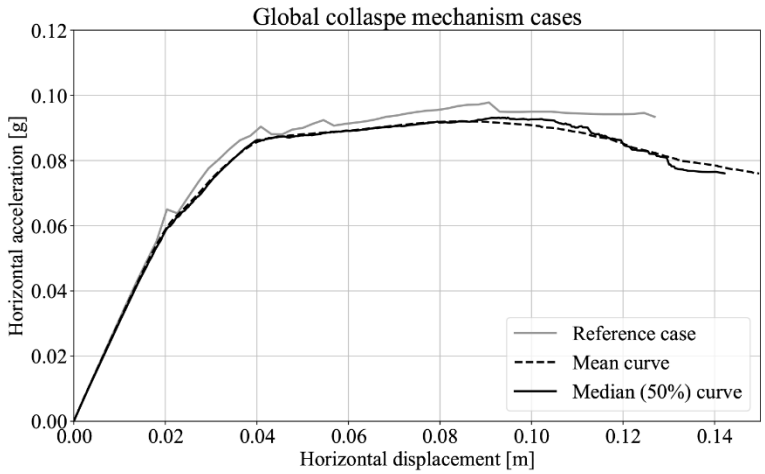

(a)

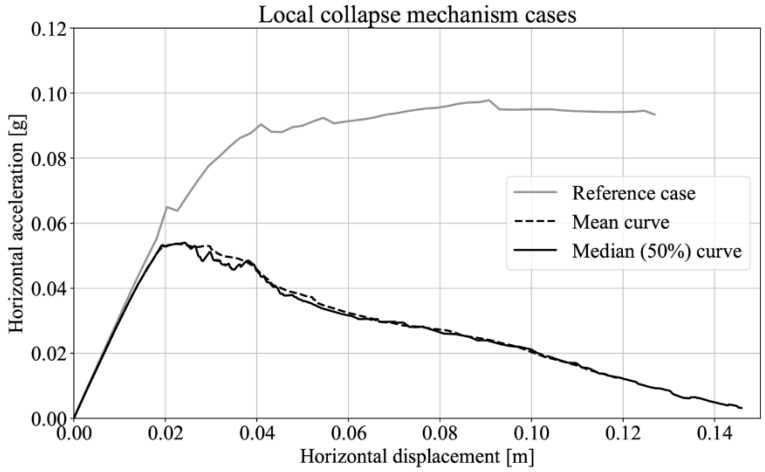

(b)

Figure 12. (a) Capacity curve of the reference model plotted with the mean and median capacity curves of the analysed cases predicting: (a) global collapse mechanism $N_G = 163$, (b) local collapse mechanism $N_L = 37$.

4.2 Seismic fragility curves

Figures 13 and 14 show the fragility curves as a function of the Peak Ground Acceleration (PGA) constructed by considering a different sample number of N in Equations (2) and (3). In the fragility curves of Figure 13 all the analysed cases have been considered, which means that N is equal to 200 in Equations (2)-(3). These graphs represent the probability that the structure will reach or exceed a considered limit state for different levels of PGA. The vertical solid line corresponds to the seismic demand of the municipality of Barcelona according to the Spanish seismic standard for a 500-year return period (Comisión Permanente de Normas Sismo resistentes, 2002), i.e. 0.04 g. For this seismic demand, and considering all the analysed cases, there is a 100% probability that the structure will reach the limit state LS_1, 50.9% probability for LS_2, 12.4% probability for LS_3 and 5.2% probability for LS_4.

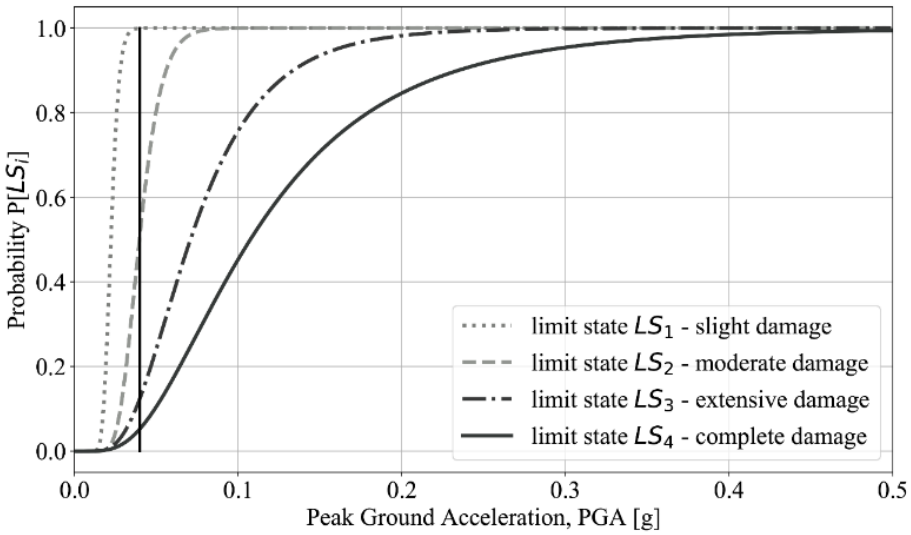

Figure 13. Fragility curves for the different limit states in terms of Peak Ground Acceleration (PGA) considering the 200 analysed cases. The vertical line corresponds to PGA = 0.04g, i.e. the seismic demand of Barcelona with a 500-year return period.

Figure 14a and Figure 14b show the fragility curves considering only the group of analyses predicting a global and a local collapse mechanism, respectively, while Table 6 summarizes the probabilities for the occurrence of each limit state. In particular, the fragility curves of Figure 14a are constructed considering only the N_G = 163 cases predicting a global mechanism of the studied macro-element for the computation of the median and lognormal standard deviation (i.e. N=N_G in Equations (2)-(3)). In the same way, the fragility curves of Figure 14b are constructed considering only the N_L = 37 cases predicting a local mechanism of the studied macro-element for the computation of the median and lognormal standard deviation (i.e. N=N_L in Equations (2)-(3)). This differentiation of the fragility curves according to the collapse mechanism shows that the cases predicting a global collapse mechanism are characterized by a much lower seismic vulnerability compared to those predicting the local collapse of the right buttress. Specifically, there is zero probability for the occurrence of limit states LS_3 and LS_4, whereas the respective probabilities for these two limit states for the local mechanism cases are 68.7% and 51.6%. The probability of limit state LS2 presents also an important difference of 39.4% between the two groups, being 50.7% for the global mechanism group and 90.1% for the local one. On the contrary, there is a 100% probability for the occurrence of the first limit state for both groups.

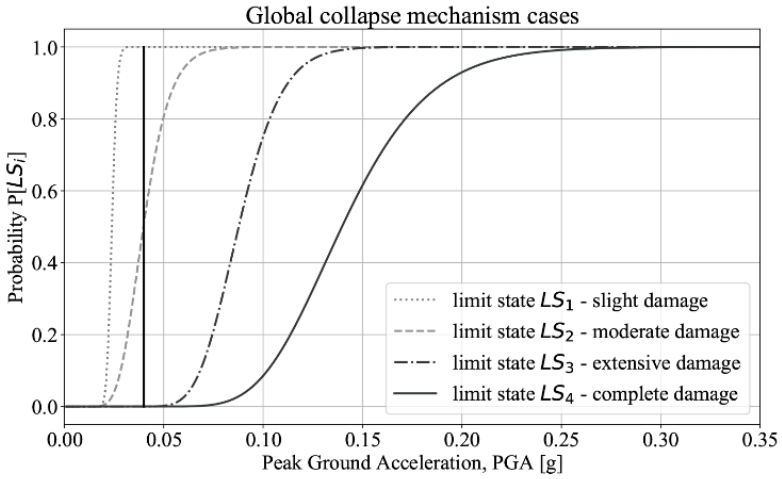

(a)

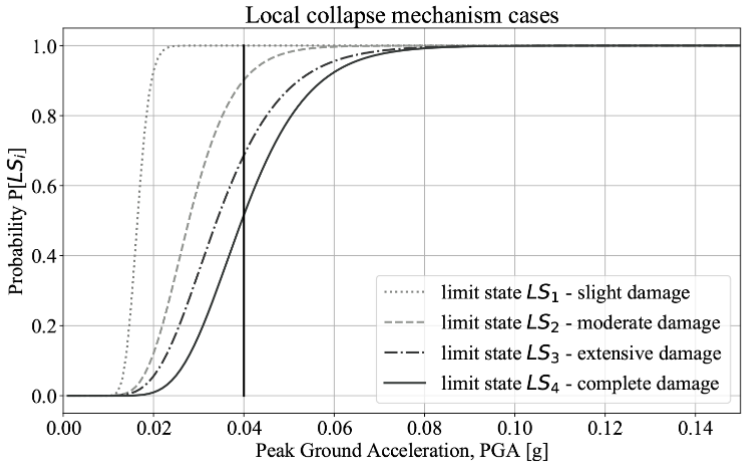

(b)

Figure 14. Fragility curves for the different limit states in terms of Peak Ground Acceleration (PGA) considering: (a) the N_G = 163 cases predicting a global collapse mechanism, (b) the N_L = 37 cases predicting a local collapse mechanism.

Another possibility for assessing the fragility of the structure is combining the fragility curves developed for each group by considering the number of cases giving each mechanism (i.e. N_G and N_L). This combined probability P_C can be formally expressed as

$$P_C[LS_i] = \frac{P_G[LS_i]\, N_G + P_L[LS_i]\, N_L}{N} \quad (4)$$

where N_G and N_L are the number of cases predicting a global and a local collapse mechanism, and $P_G[LS_i]$ and $P_L[LS_i]$ are the probabilities of reaching a limit state LS_i by considering only the N_G and N_L cases, respectively. The last column of Table 6 presents the combined probabilities $P_C[LS_i]$ derived from Equation (4) for each limit state. It is evident that Equation (4) gives higher predictions for the probability of all the limit states than those predicted using the total number of the analysed cases (i.e. $P[LSi]$ in the 6th column of Table 6). The only exception is given by limit state LS$_1$ that is satisfied by all analysed cases. This difference implies that in complex historical structures presenting distinct collapse mechanisms, as the one studied in this research, the use of all the results for obtaining the fragility of the structure may underestimate the vulnerability of the analysed structure. The results of the two approaches used for the estimation of the seismic fragility of the structure can be appreciated in the histograms of Figure 15.

Table 6. Probabilities for each limit state considering: the N_L cases predicting a local mechanism (columns 2 and 3), the N_G cases predicting a global collapse mechanism (columns 4 and 5) and all the cases N (columns 5 and 6).

Limit State	$P_L[LS_i]$	$P_L[LS_i]\frac{N_L}{N}$	$P_G[LS_i]$	$P_G[LS_i]\frac{N_G}{N}$	$P[LS_i]$	$P_C[LS_i]$
LS$_1$	100	18.5	100	81.5	100	100
LS$_2$	90.1	16.7	50.7	41.3	50.9	58
LS$_3$	68.7	12.7	0	0	12.4	12.7
LS$_4$	51.6	9.5	0	0	5.2	9.5

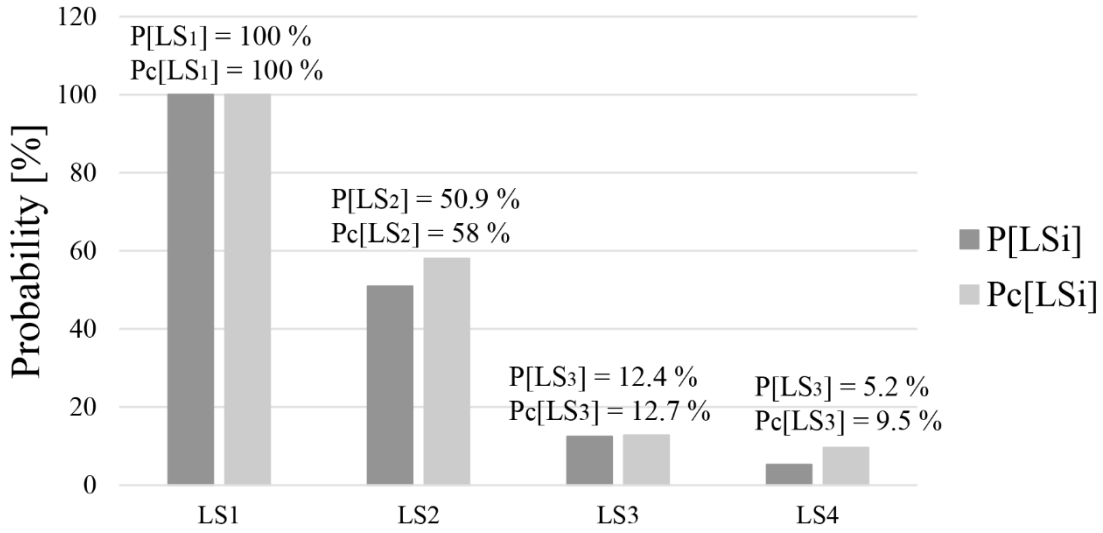

Figure 15. Probability of each limit state by considering all the cases ($P[LS_i]$), and by considering the weighted cases giving the two different mechanisms ($P_c[LS_i]$).

Figures 16 and 17 illustrate the damage corresponding to the four limit states for a global and a local collapse mechanism case, respectively. In the following, the probabilities for each limit state correspond to column 3 of Table 6 for the local mechanism group and to column 5 of Table 6 for the global mechanism group. Considering the cases predicting a global collapse mechanism, the first limit state LS_1 with a probability of 81.5%, corresponds to cracking at the lateral naves and at the bottom of the right buttress (Figure 16a). The second limit state LS_2 has a probability of 41.3% and corresponds to further propagation of the damage in the lateral aisles and initiation of cracking at the central nave (Figure 16b). The last two limit states LS_3 and LS_4 are characterized by the propagation of damage at all the naves and the two buttresses and have a 0% probability (Figure 16c-d).

Considering the local collapse mechanism, the first limit state LS_1 has 100% of probability and corresponds to damage at the buttresses above the vaults of the lateral naves and initiation of cracking at the two buttresses (Figure 17a). For the second limit state LS_2 (16.7% probability) there is already important shear cracking at the right buttress (Figure 17b). The cracks present in LS_2 increase their propagation in the third limit state LS_3 (probability 12.7%) as no important new damage occurs in the structure (Figure 17c). Finally, the last limit state LS_4 (probability 9.5 %) corresponds to the shear failure of the right buttress (Figure 17d).

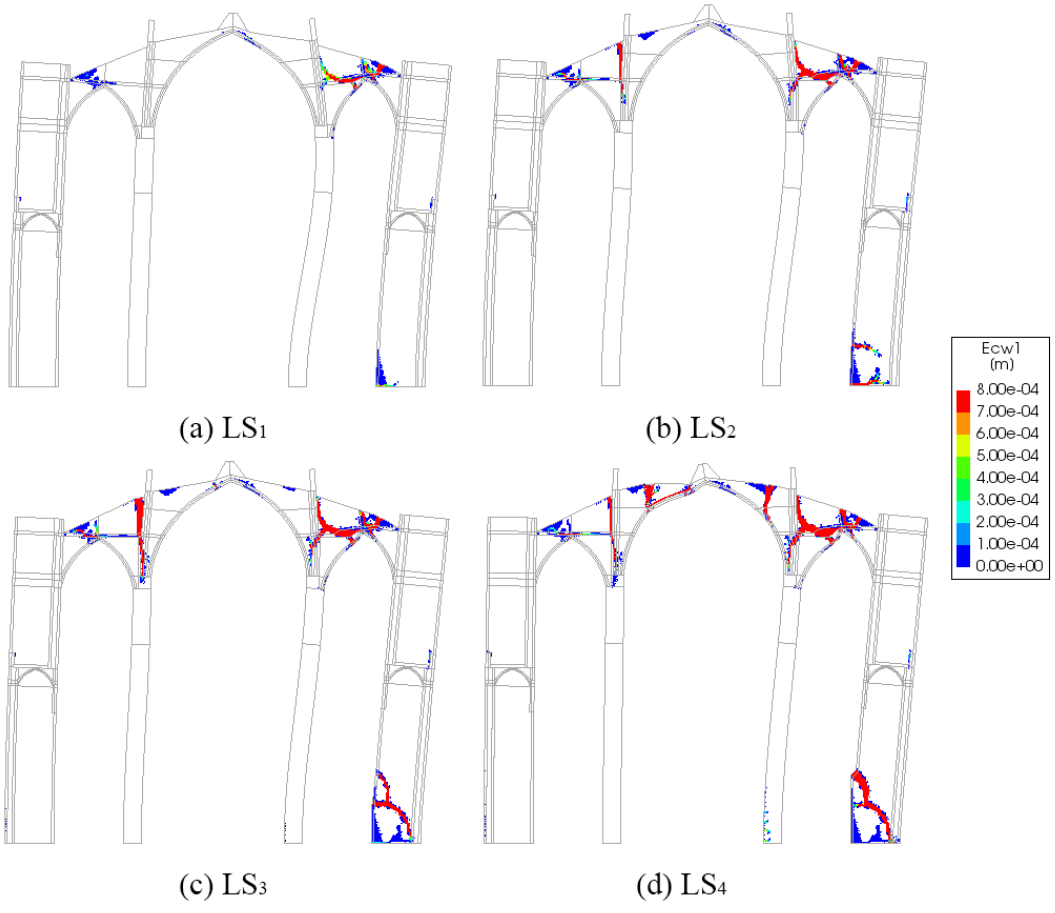

Figure 16. Crack width and distribution for an analysed case predicting a global collapse mechanism corresponding to the four considered limit states (a) LS_1, (b) LS_2, (c) LS_3, and (d) LS_4.

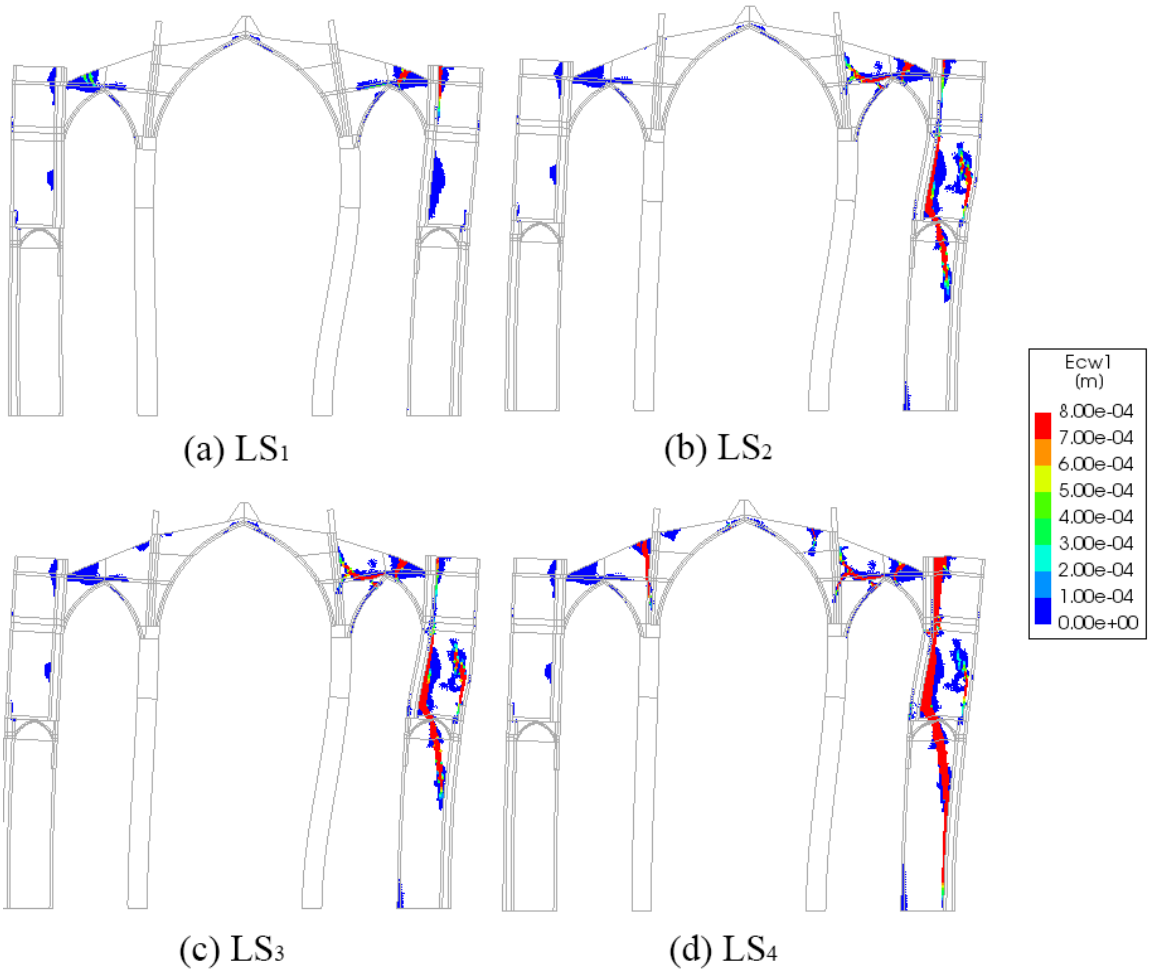

Figure 17. Crack width and distribution for an analysed case predicting a local collapse mechanism corresponding to the four considered limit states: (a) LS_1, (b) LS_2, (c) LS_3, and (d) LS_4.

Considering the above results, as well as the fragility of the structure presented in Table 6, the most vulnerable parts of the building are the lateral naves and the top portions of the buttresses, since they are expected to experience damage for the expected seismic hazard in Barcelona for a 500-year return period (PGA = 0.04 g).

4.3 Effect of the sample size choice

This section investigates the effect of the sample size on the performed probabilistic analysis through a convergence study of the Monte Carlo simulation based on the approach presented in (Ballio and Guadagnini, 2004). The metrics used for the determination of the convergence are the median (θ_{LS_i} Equation (2)) and the standard deviation of the lognormal distribution (β_{LS_i} Equation (3)) of the PGA for each limit state, since these two statistical measures are used in the definition of the fragility curves in Equation (1).

Figure 18 presents the variation of the above median and standard deviation values for each limit state as a function of the sample size *N*. These figures have been prepared by considering 200 Monte Carlo simulations with an increasing sample size from $N = 10$ up to $N=200$, i.e. by changing the sample size in Equations (2) and (3). The values of these two statistical measures converge faster for the first two limit states (LS_1 & LS_2) compared to the last two (LS_3 & LS_4). This is because the last two limit states are defined considering the ultimate displacement of the structure (see Table 6), which has been considered the one corresponding to 80% of the maximum capacity of the structure. Due to this, the computed PGAs for LS_3 & LS_4 depend heavily on the post-peak response of each analysed case, which as can be seen in Figure 9 can vary significantly. This variation is related not only to the different material properties of each analysis, but also to numerical aspects such as the convergence strategy, the used constitutive model and the finite element technology (Vlachakis *et al.*, 2019). For this reason, the median and standard deviation of LS_3 & LS_4 present a slower convergence, characterized by an oscillating trend around a constant value for a sample size above 100. In particular, considering the case of LS_4, there is a 9% difference between the maximum and the minimum reported values

of the standard deviation for sample sizes above 100. For the median value of LS_4, this difference is limited to 3%. Considering the above results, the two statistical measures used in the definition of the fragility curves start converging for a sample number N>100. Therefore, the chosen sample size of N=200 seems to be appropriate for the selected case study.

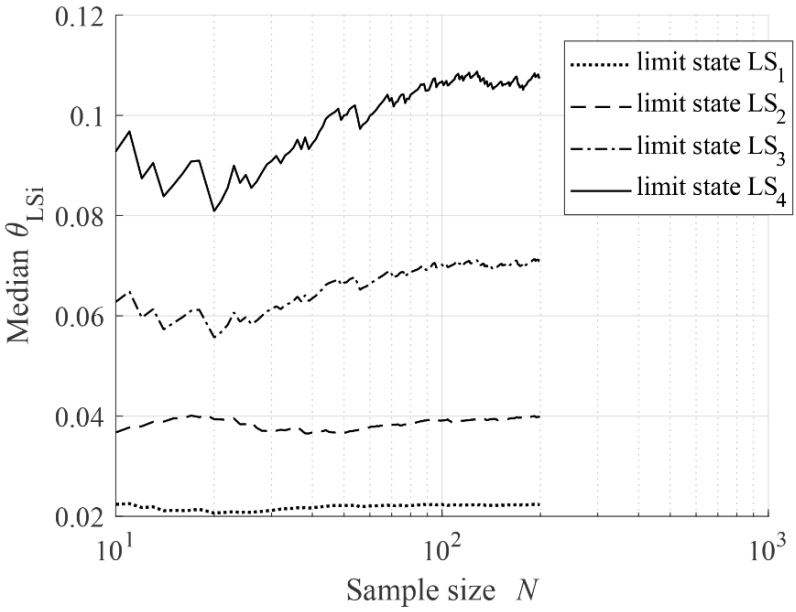

(a)

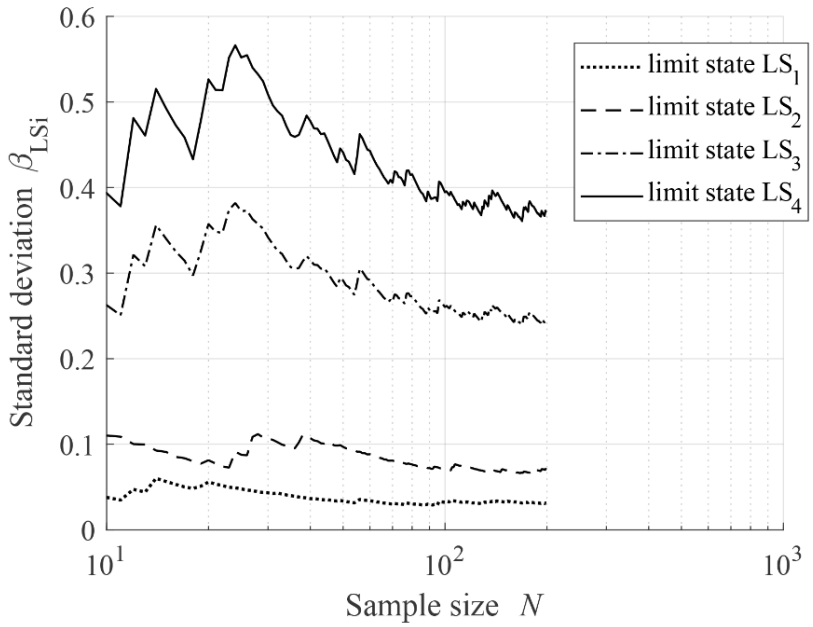

(b)

Figure 18. Effect of the sample size N of the Monte Carlo Simulations: convergence of the median θ_{LS_i} (a) and standard deviation β_{LS_i} (b) of the PGA necessary for producing each limit state for the seismic demand of the city of Barcelona.

5. Conclusions

This work has presented a methodology for the probabilistic seismic assessment of complex masonry structures including the analysis of the uncertainty related to the material properties. The proposed method is based on the development of a stochastic nonlinear analysis through Monte Carlo simulation, together with the use of the Finite Element method for the seismic analysis of the masonry structure. The proposed approach has been used to investigate the seismic fragility of the representative bay structure of the church of Santa Maria del Mar in Barcelona under earthquakes acting in its transverse

direction. An important outcome of the work is the proposal of seismic fragility curves for the representative bay structure of this valuable heritage monument.

The application of the proposed probabilistic methodology has shown its ability to identify different damage and collapse mechanisms that might be overlooked in conventional approaches based on a deterministic/semi-probabilistic evaluation of the material properties. The probabilistic seismic assessment procedure has demonstrated that the seismic response of complex masonry structures, such as historical churches and cathedrals, may show a significant sensitivity to the variation of the material properties and thus to the uncertainty linked to them. The use of the proposed method allows a more accurate evaluation of the seismic safety of the building compared to the conventional deterministic/semi-probabilistic approaches.

The adopted methodology predicts that two collapse mechanisms are possible for the analysed macro-element of the church of Santa Maria del Mar. The first one is a global collapse mechanism, predicted by 81.5% of the analysed cases, with cracking in the main and lateral naves and the lateral buttresses. The second collapse mechanism, predicted by 18.5% of the analysed cases, is characterized by the local failure of the lateral buttress due to shear cracking. The seismic fragility of the structure depends importantly on the final collapse mechanism. The cases resulting in the global collapse of the structure present low seismic fragility for the seismic demand of the city of Barcelona, and only slight and moderate damage states are probable. On the contrary, the cases with a local collapse mechanism present low capacity and a very brittle post-peak response resulting in a high seismic fragility, which exceeds 50% for all the investigated limit states.

Taking into account the mentioned distinct collapse mechanisms and structural responses, the seismic fragility of all the analysed cases has been investigated using two approaches. In the first one, the fragility curves have been determined using all the analysed cases without making any distinction between those predicting a local and a global collapse mechanism. In the second one, the probability of having a different collapse mechanism is considered by assigning specific weights to the cases predicting a local and a global collapse mechanism. The latter differentiation results in increased levels for the seismic fragility of the investigated structure for all the limit states.

The main aim of this work is to contribute to the discussion on the possibility to apply probabilistic approaches for the seismic assessment of complex historical masonry structures in which a complete knowledge of the material properties is difficult. The presented results open new potential lines of research for the probabilistic seismic assessment of historical masonry structures, such as the study of the effect of the uncertainty related to the seismic hazard or the geometry of structural members. The study carried out on the representative bay structure of Santa Maria del Mar church in Barcelona encourages the possibility of investigating the seismic vulnerability of additional macro-elements of the same structure and the use of more complex 3D models. At the same time, it emerges the need for a definition of specific seismic damage limit states specifically associated with different structural typologies of irregular masonry structures (e.g. churches, cathedrals, palaces), beside the already investigated case of common masonry buildings. As for the proposed methodology based on Monte Carlo stochastic simulation, specific issues requiring further research are those related to the analysis of the effect of the sample size

for different typologies of historical structures. To this end, the choice of different sampling strategies (e.g. Latin Hypercube Sampling, orthogonal sampling) can improve the efficiency of the sampling process.

Acknowledgements

This research has received the financial support from the Ministry of Economy and Competitiveness and from the Ministry of Science, Innovation and Universities of the Spanish Government, as well as that of the ERDF (European Regional Development Fund) through projects MULTIMAS (Multiscale techniques for the experimental and numerical analysis of the reliability of masonry structures, ref. num. BIA2015-63882-P) and SEVERUS (Multilevel evaluation of seismic vulnerability and risk mitigation of masonry buildings in resilient historical urban centres, ref. num. RTI2018-099589-B-I00). The work was supported by the European Union within the framework of the Erasmus Mundus Advanced Master in Structural Analysis of Monuments and Historical Constructions (SAHC).

The authors would like to acknowledge Prof. Sergio Lagomarsino for the fruitful discussions after the presentation of the research during the SAHC 2018 conference in Cusco, Perú.

References

Acito, M. *et al.* (2014) 'Collapse of the clock tower in Finale Emilia after the May 2012 Emilia Romagna earthquake sequence: Numerical insight', *Engineering Structures*. Elsevier Ltd, 72(May 2012), pp. 70–91. doi: 10.1016/j.engstruct.2014.04.026.

Atamturktur, S., Hemez, F. M. and Laman, J. A. (2012) 'Uncertainty quantification in model verification and validation as applied to large scale historic masonry monuments', *Engineering Structures*. doi: 10.1016/j.engstruct.2012.05.027.

ATC-58 (2009) *Guidelines for Seismic Performance Assessment of Buildings, Applied Technology Council*. Redwood City, California.

Ballio, F. and Guadagnini, A. (2004) 'Convergence assessment of numerical Monte Carlo simulations in groundwater hydrology', *Water Resources Research*, 40(4), pp. 1–5. doi: 10.1029/2003WR002876.

Bartoli, G. *et al.* (2017) 'Bayesian model updating of historic masonry towers through dynamic experimental data', in *Procedia Engineering*. doi: 10.1016/j.proeng.2017.09.267.

Bažant, Z. P. and Oh, B. (1983) 'Crack band theory for fracture of concrete', *Materials and Structures*, 16, pp. 155–177. doi: 10.1007/BF02486267.

Bosiljkov, V., D'Ayala, D. and Novelli, V. (2015) 'Evaluation of uncertainties in determining the seismic vulnerability of historic masonry buildings in Slovenia: use of macro-element and structural element modelling', *Bulletin of Earthquake Engineering*. doi: 10.1007/s10518-014-9652-7.

Bracchi, S. *et al.* (2015) 'Consideration of modelling uncertainties in the seismic

assessment of masonry buildings by equivalent-frame approach', *Bulletin of Earthquake Engineering*. doi: 10.1007/s10518-015-9760-z.

Bracchi, S. *et al.* (2016) 'Seismic assessment of masonry buildings accounting for limited knowledge on materials by Bayesian updating', *Bulletin of Earthquake Engineering*. doi: 10.1007/s10518-016-9905-8.

Castellazzi, G. *et al.* (2017) 'An innovative numerical modeling strategy for the structural analysis of historical monumental buildings', *Engineering Structures*. Elsevier Ltd, 132, pp. 229–248. doi: 10.1016/j.engstruct.2016.11.032.

CEB-FIP (2013) *Model Code for Concrete Structures 2010, Model Code for Concrete Structures 2010*. Comite Euro-International Du Beton. doi: 10.1002/9783433604090.

CNR-DT 212/2013 (2014) *Guide for the Probabilistic Assessment of the Seismic Safety of Existing Buildings*. Rome, Italy.

Comisión Permanente de Normas Sismo resistentes (2002) *Norma de construcción sismo resistente NCSE-02, Real Decreto 997/2002, Spanish Ministry of Public Works, Madrid, Spain, 2002 [in Spanish]*. Madrid, Spain.

Contrafatto, F. R. (2017) *Vulnerability assessment of monumental masonry structures including uncertainty*. Universitat Politècnica de Catalunya.

D'Ayala, D. F. and Ansal, A. (2012) 'Non linear push over assessment of heritage buildings in Istanbul to define seismic risk', *Bulletin of Earthquake Engineering*, 10(1), pp. 285–306. doi: 10.1007/s10518-011-9311-1.

EN 1998-1 (Eurocode 8) (2003) 'Design of structures for earthquake resistance, Part 1 General rules seismic actions and rules for buildings'.

Fajfar, P. (1999) 'Capacity spectrum method based on inelastic demand spectra',

Earthquake Engineering & Structural Dynamics. John Wiley & Sons, Ltd., 28(9), pp. 979–993. doi: 10.1002/(SICI)1096-9845(199909)28:9<979::AID-EQE850>3.0.CO;2-1.

Federal Emergency Management Agency (2010) *HAZUS-MH MR4: Technical Manual, Vol. Earthquake Model*. Washington DC.

Fontserè, E. (1971) 'Recopilació de dades sísmiques de les terres catalanes entre 1100 i 1906'. Barcelona: Generalitat de Catalunya.

Franchin, P. *et al.* (2018) 'Modelling Uncertainties of Italian Code- Conforming Structures for the Purpose of Seismic Response Analysis Modelling Uncertainties of Italian Code-Conforming Structures for the Purpose of Seismic Response Analysis', *Journal of Earthquake Engineering*. Taylor & Francis, 00(00), pp. 1–26. doi: 10.1080/13632469.2018.1527262.

Franchin, P., Pinto, P. E. and Rajeev, P. (2010) 'Confidence Factor?', *Journal of Earthquake Engineering*, 14(7), pp. 989–1007. doi: 10.1080/13632460903527948.

González, R. *et al.* (2008) 'Construction process, damage and structural analysis. Two case studies.', in D'Ayala, D. and Fodde, E. (eds) *Structural analysis of historic construction: preserving safety and significance*. Bath: CRC Press, pp. 643–651.

Graf, W., Götz, M. and Kaliske, M. (2015) 'Analysis of dynamical processes under consideration of polymorphic uncertainty', *Structural Safety*. doi: 10.1016/j.strusafe.2014.09.003.

Irizzary, I. P. (2004) *An advanced approach to seismic risk assessment. Application to the cultural heritage and the urban system of Barcelona*. Universitat Politècnica de Catalunya (UPC-BarcelonaTech).

Jalayer, F., Iervolino, I. and Manfredi, G. (2010) 'Structural modeling uncertainties and

their influence on seismic assessment of existing RC structures', *Structural Safety*. Elsevier Ltd, 32(3), pp. 220–228. doi: 10.1016/j.strusafe.2010.02.004.

Lagomarsino, S. and Cattari, S. (2014a) 'Fragility Functions of Masonry Buildings', in Pitilakis, K., Crowley, H., and Kaynia, A. (eds) *SYNER-G: Typology Definition and Fragility Functions for Physical Elements at Seismic Risk*. Springer, pp. 111–156. doi: 10.1007/978-94-007-7872-6_5.

Lagomarsino, S. and Cattari, S. (2014b) 'PERPETUATE guidelines for seismic performance-based assessment of cultural heritage masonry structures', *Bulletin of Earthquake Engineering*, 13(1), pp. 13–47. doi: 10.1007/s10518-014-9674-1.

Lagomarsino, S. and Giovinazzi, S. (2006) 'Macroseismic and mechanical models for the vulnerability and damage assessment of current buildings', *Bulletin of Earthquake Engineering*, 4(4), pp. 415–443. doi: 10.1007/s10518-006-9024-z.

Lagomarsino, S. and Resemini, S. (2009) 'The Assessment of Damage Limitation State in the Seismic Analysis of Monumental Buildings', *Earthquake Spectra*, 25(2), pp. 323–346. doi: 10.1193/1.3110242.

Lourenço, P. B. (2009) 'Recent Advances in Masonry Modelling: Micromodelling and Homogenisation', in *Multiscale Modeling in Solid Mechanics: computational approaches*, pp. 251–294. doi: 10.1142/9781848163089_0006.

Mayer, P. (2008) *Barcelona, Església de Santa Maria del Mar-PM 15932, Wikimedia Commons*. Available at: https://commons.wikimedia.org/wiki/File:Barcelona,_Església_de_Santa_Maria_del_Mar-PM_15932.jpg.

MIT (2009) *Ministero delle Infrastrutture e dei Transporti (M.I.T) Circolare 2 febbraio*

2009, n. 617, Istruzioni per l'applicazione delle ``Nuove norme tecniche per le costruzioni'' di cui al decreto ministeriale 14 gennaio 2008. Rome, Italy.

Mouroux, P. and Le Brun, B. (2006) 'Presentation of RISK-UE project', *Bulletin of Earthquake Engineering*, 4(4), pp. 323–339. doi: 10.1007/s10518-006-9020-3.

Murcia, J. (2008) *Seismic Analysis of Santa Maria del Mar Church in Barcelona*. Universitat Politècnica de Catalunya.

Ortega, J. *et al.* (2018) 'Assessment of the efficiency of traditional earthquake resistant techniques for vernacular architecture', *Engineering Structures*. Elsevier, 173(February), pp. 1–27. doi: 10.1016/j.engstruct.2018.06.101.

Pagnini, L. C. *et al.* (2011) 'A mechanical model for the seismic vulnerability assessment of old masonry buildings', *Earthquakes and Structures*. Techno-Press, 2(1), pp. 25–42. doi: 10.12989/eas.2011.2.1.025.

Parisi, F. and Augenti, N. (2012) 'Uncertainty in Seismic Capacity of Masonry Buildings', *Buildings*. doi: 10.3390/buildings2030218.

Park, J. *et al.* (2009) 'Seismic fragility analysis of low-rise unreinforced masonry structures', *Engineering Structures*. Elsevier Ltd, 31(1), pp. 125–137. doi: 10.1016/j.engstruct.2008.07.021.

Pelà, L. *et al.* (2016) 'Analysis of the Effect of Provisional Ties on the Construction and Current Deformation of Mallorca Cathedral', *International Journal of Architectural Heritage*. Taylor & Francis, 10(4), pp. 418–437. doi: 10.1080/15583058.2014.996920.

Petromichelakis, Y., Saloustros, S. and Pelà, L. (2014) 'Seismic assessment of historical masonry construction including uncertainty', in Cunha, Á. et al. (eds) *9th International Conference on Structural Dynamics, EURODYN 2014*. Porto, Portugal, pp. 297–304.

Roca, P. *et al.* (2009) *Assessment and strengthening of historical stone masonry structures subjected to seismic action*. Mostar, Bosnia and Herzegovina: Proceedings of the ISCARSAH Symposium Mostar-09, 12th July 2009.

Roca, P. *et al.* (2013) 'Continuum FE models for the analysis of Mallorca Cathedral', *Engineering Structures*. Elsevier Ltd, 46, pp. 653–670. doi: 10.1016/j.engstruct.2012.08.005.

Rota, M., Penna, A. and Magenes, G. (2010) 'A methodology for deriving analytical fragility curves for masonry buildings based on stochastic nonlinear analyses', *Engineering Structures*. Elsevier Ltd, 32(5), pp. 1312–1323. doi: 10.1016/j.engstruct.2010.01.009.

Rota, M., Penna, A. and Magenes, G. (2014) 'A framework for the seismic assessment of existing masonry buildings accounting for different sources of uncertainty', *Earthquake Engineering and Structural Dynamics*. doi: 10.1002/eqe.2386.

Saloustros, S. *et al.* (2014) 'Numerical analysis of structural damage in the church of the Poblet monastery', *Engineering Failure Analysis*. Elsevier Ltd, 48, pp. 41–61. doi: 10.1016/j.engfailanal.2014.10.015.

Saloustros, S. *et al.* (2019) 'Vulnerability Assessment of Monumental Masonry Structures Including Uncertainty', in Aguilar, R. et al. (eds) *Structural Analysis of Historical Constructions - An interdisciplinary approach*. Springer, Cham, pp. 1219–1228. doi: 10.1007/978-3-319-99441-3_131.

Simões, A. *et al.* (2015) 'Fragility curves for old masonry building types in Lisbon', *Bulletin of Earthquake Engineering*, 13(10), pp. 3083–3105. doi: 10.1007/s10518-015-9750-1.

Snoj, J. and Dolšek, M. (2011) ‘Simplified probabilistic seismic performance assessment of masonry buildings with consideration of aleatoric and epistemic uncertainties’, in *Proceedings of the 8th International Conference on Structural Dynamics, EURODYN 2011*.

Sykora, M. and Holicky, M. (2010) ‘Probabilistic model for masonry strength of existing structures’, *Engineering Mechanics*, 17(1), pp. 61–70.

TNO (2017) ‘DIsplacement method ANAlyser (DIANA FEA), release 10.1, Delft, Netherlands’. Delft, Netherlands.

Tondelli, M. *et al.* (2012) ‘Evaluation of Uncertainties in the Seismic Assessment of Existing Masonry Buildings’, *Journal of Earthquake Engineering*, 16(sup1), pp. 36–64.

Vamvatsikos, D. and Fragiadakis, M. (2010) ‘Incremental dynamic analysis for estimating seismic performance sensitivity and uncertainty’, *Earthquake Engineering & Structural Dynamics*, 39, pp. 141–163. doi: 10.1002/eqe.935.

Vanin, F. *et al.* (2017) ‘Estimates for the stiffness , strength and drift capacity of stone masonry walls based on 123 quasi-static cyclic tests reported in the literature’, *Bulletin of Earthquake Engineering*. Springer Netherlands, (August). doi: 10.1007/s10518-017-0188-5.

Vendrell, M. *et al.* (2007) *La Basílica de Santa Maria del Mar. Study of the construction and history, construction materials and structural stability*. (in Catalan).

Vlachakis, G. *et al.* (2019) ‘Out-of-plane seismic response and failure mechanism of masonry structures using finite elements with enhanced strain accuracy’, *Engineering Failure Analysis*. Pergamon, 97, pp. 534–555. doi: 10.1016/J.ENGFAILANAL.2019.01.017.